JACS
JOURNAL OF THE AMERICAN CHEMICAL SOCIETY
Article
pubs.acs.org/JACS

Using TiO_2 as a Conductive Protective Layer for Photocathodic H_2 Evolution

Brian Seger,[†] Thomas Pedersen,[‡] Anders B. Laursen,[†] Peter C. K. Vesborg,[†] Ole Hansen,[‡] and Ib Chorkendorff*[,†]

[†]Department of Physics, CINF, and [‡]Department of Micro- and Nanotechnology, Technical University of Denmark, DK-2800, Kongens Lyngby, Denmark

Supporting Information

ABSTRACT: Surface passivation is a general issue for Si-based photoelectrodes because it progressively hinders electron conduction at the semiconductor/electrolyte interface. In this work, we show that a sputtered 100 nm TiO_2 layer on top of a thin Ti metal layer may be used to protect an n^+p Si photocathode during photocatalytic H_2 evolution. Although TiO_2 is a semiconductor, we show that it behaves like a metallic conductor would under photocathodic H_2 evolution conditions. This behavior is due to the fortunate alignment of the TiO_2 conduction band with respect to the hydrogen evolution potential, which allows it to conduct electrons from the Si while simultaneously protecting the Si from surface passivation. By using a Pt catalyst the electrode achieves an H_2 evolution onset of 520 mV vs NHE and a Tafel slope of 30 mV when illuminated by the red part (λ > 635 nm) of the AM 1.5 spectrum. The saturation photocurrent (H_2 evolution) was also significantly enhanced by the antireflective properties of the TiO_2 layer. It was shown that with proper annealing conditions these electrodes could run 72 h without significant degradation. An Fe^{2+}/Fe^{3+} redox couple was used to help elucidate details of the band diagram.

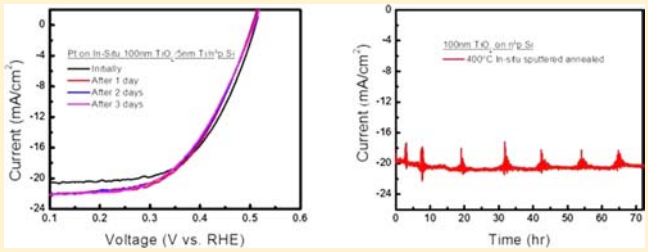

INTRODUCTION

While it has been shown that solar energy has the potential to provide enough energy for society,[1,2] there is always the issue of the intermittency of solar power. One of the most logical approaches to resolving this issue is to store this solar energy in a molecular form, such as hydrogen. Using water as a hydrogen source allows for an almost unlimited amount of hydrogen to be stored. A simple solution to solar-based hydrogen production would be to use the electricity from a solar cell in an electrolyzer to produce hydrogen. A major issue with this approach is that two devices are needed. If solar energy could be directly converted to hydrogen, only a single device would be needed. Given that the cost of the "balance of system" is typically quite large in these devices,[3] using a single system has the potential to be much more cost-effective than the two-device solar cell−electrolyzer system.

There are two major approaches to direct photocatalytic water-splitting.[4] The first approach is to find a single material that has its band structure aligned properly for both the hydrogen evolution and the water oxidation reaction. This approach has the advantage of simplicity and the fact that most of these materials are quite durable oxides.[5] The second approach is to find two different photoabsorbers that when put together have the right band alignments to split water.[2,6] Using two materials allows for each material to have a much smaller band gap than in the first approach. This is because in the second approach the two materials combined need to the give the same photovoltage as the single material in the first approach. It has been shown that the two-photoabsorber approach theoretically has the ability to give a higher maximum photocatalytic water-splitting efficiency.[7,8]

Furthermore, recent theoretical work has shown that silicon has one of the best band gaps and band alignments for the photocathode of a two-photoabsorber water-splitting device.[9] However, one of the major limitations with silicon is that it quite easily oxidizes in acidic solution and deactivates due to the electrically insulating properties of SiO_2.[6] Other potential photoabsorbers (such as CdS, GaP, Cu_2O) on the cathode side also face similar issues. The Lewis group has started working on protecting Si using organic functional groups;[10,11] however, water-splitting devices should last for decades, and it is not known whether these organics can remain protective for that long.

In our previous work on the photocathodic H_2 evolution reaction, we showed that titanium metal also has the potential to work as a protecting layer.[12] During short-term tests (1 h) the titanium is relatively stable; however, longer term test results show that the titanium fails [see Supporting Information (SI), Figure S1]. Thus, an approach must be found to make this a more durable support. Another issue when using titanium as a protective layer is that titanium metal has a native oxide, which is semiconducting. While the oxide layer is initially thin, over

Received: October 1, 2012
Published: January 4, 2013

   dx.doi.org/10.1021/ja309523t | J. Am. Chem. Soc. 2013, 135, 1057−1064

time the depth of the oxidation will slowly increase. Since commercially viable water-splitting devices need to be durable for years if not decades, a significant oxide layer will develop that must be accounted for. Thus, a more realistic protective layer to study would be TiO_2, rather than titanium. By using TiO_2 as a protection layer, an important question remains, namely, how efficiently can electrons travel through this semiconductor to the electrolyte? In this work, we show that, under photocatalytic water-splitting conditions, TiO_2 provides negligible impediment for electron transfer from the photocathode to the electrolyte. Building on the pioneering work by the Bard group,[13] we use an Fe(III)/Fe(II) redox couple we further show that the reason for the efficient electron transfer through TiO_2 is likely due to the close alignment with the H_2 evolution reaction and the conduction band in TiO_2. We also show that proper annealing of the TiO_2 is the key to long-term durability.

RESULTS AND DISCUSSION

Photocathodic H_2 Evolution Efficiency. To produce the photocathodes, p-type Si wafers were first doped with a thin n^+ doping using previous methods.[12] This n^+ doping isolates the band-bending to within the silicon, which allows for increased photovoltage for the hydrogen evolution reaction.[14] For a standard electrode, Pt was then sputtered on the n^+p Si. For Ti-based photocathodes, 5 nm of titanium was sputtered on n^+p Si samples and various amounts of TiO_2 were reactive-sputtered on top. The thin layer of titanium was important because it prevented inadvertent silicon oxidation from the reactive sputtering used for TiO_2 deposition. At this point in the photocathode fabrication some samples were annealed in either vacuum or air at 400 °C for 90 min with a ramp rate of 10 °C/min, while others were left unannealed.

Using previous methods,[12] electrodes were made for photoelectrochemical testing. All samples were cleaned with piranha solution and washed, and the Ti-coated electrodes then had 250 ng (Pt basis) of a dinitrosulfatoplatinate solution drop-cast on them. In the case of the n^+p Si with no metal, the sample was etched in 1% HF for 1 min and then washed with water before Pt salt deposition. The samples were irradiated with the red part (λ > 635 nm) of a simulated AM 1.5 spectrum to appropriately approximate the wavelengths and intensity this electrode would receive in a real two-photon device.[6] An initial cyclic voltammogram (CV) scan of all electrodes reduced the Pt salt to Pt metal, and successive scans were used for H_2 evolution CV's. Figure 1 shows the cyclic voltammogram for photocatalytic H_2 evolution of the various n^+p Si electrodes. H_2 could be visually observed bubbling off of all samples as the current increased. This bubbling has been verified to be hydrogen gas.[12]

All of these electrodes have onset potentials well in excess of the H^+/H_2 redox potential, indicating that these systems are good candidates for the photocathodic side of a two-photon water-splitting device. The Pt on n^+p Si has an onset of 0.51 V vs RHE under these conditions, while all the Ti-protected electrodes have a slightly higher open circuit voltage at 0.52 V vs RHE, which could be due to lower surface recombination for the Ti-protected cathode. What is more impressive, however, is that the photogenerated electron in the Si appears to travel through the TiO_2 with negligible ohmic resistance or loss in onset potential. It was determined that the Tafel slopes for the HER on the Pt/100 nm TiO_2/5 nm Ti/n^+p Si electrodes were 30 mV/decade without correction for ohmic loss. The Tafel slope for pure Pt is normally 30 mV/decade, thus indicating that ohmic losses are negligible. As will be discussed later, the key to the electron transfer is that the electron can conduct through the TiO_2 conduction band to the Pt catalyst.

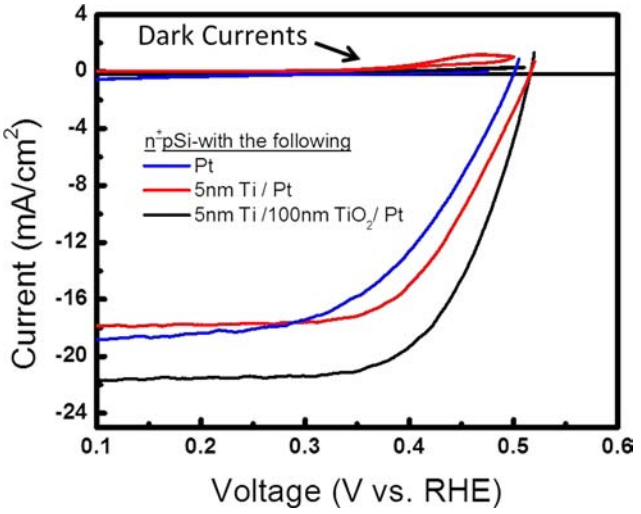

Figure 1. CV scans of photoelectrodeposited Pt on various n^+p Si electrodes. The samples were irradiated with the red part (λ > 635 nm) of a simulated AM1.5 spectrum and scanned at 50 mV/s in a H_2-saturated 1 M $HClO_4$ electrolyte.

One important property of TiO_2 is that it is known to work as an antireflective coating.[15] This effect is quite prominent in Figure 1, resulting in a higher saturation current for the 100 nm TiO_2/5 nm Ti samples compared to the samples with only 5 nm Ti. It should be noted that even though 5 nm of Ti was sputtered on these samples, Ti forms a native oxide layer of ~3 nm;[16] thus, the actual Ti left that could potentially absorb light was quite minimal. Since the ultimate purpose of this study is to use silicon in a two-photon water-splitting device, Si will only absorb long wavelength light in actual devices.[8] It was determined that the IPCE was near 90% for irradiation at long wavelengths (SI, Figure S2)

In Figure 1, the TiO_2 was sputtered at room temperature. In the Supporting Information (Figure S3), variations of the deposition procedure were tested. (Figure 2b and c also show this data, but in a different context.) These results show that the sputtered TiO_2 followed by 400 °C annealing in a vacuum has similar CV's to the TiO_2 deposited in Figure 1. Depositing at room temperature and then annealing in air, however, showed a similar onset, but a worse slope. This was attributed to the oxygen from air partially oxidizing the underlying Si. In situ deposition of the TiO_2 at 400 °C also worked, but the CV was slightly worse in this case. This can most probably be attributed to the thickness of the Ti metal interlayer being insufficient to prevent slight silicon oxidation. While the cyclic voltammograms of different deposition methods are relatively uninteresting, durability studies show a vast difference between the deposition methods.

Durability Studies. It was found that samples with TiO_2 coatings could be pulled in and out of electrolytes multiple times with no noticeable change in performance, while samples with H-terminated Si would oxidize and become inactive the first time they were pulled out of the electrolyte.[6] To further investigate the durability of the Pt/100 nm TiO_2/5 nm Ti/n^+p Si samples, they were tested up to 24 h. An n^+p Si electrode with 5 nm of sputtered Pt was also tested as a standard. Figure 2a shows the results of samples that were unannealed (UA) or either annealed at 400 °C for 90 min in a vacuum (VA) or air (AA). The 400 °C in-situ sputter annealed samples are also shown on this figure

dx.doi.org/10.1021/ja309523t | J. Am. Chem. Soc. 2013, 135, 1057−1064

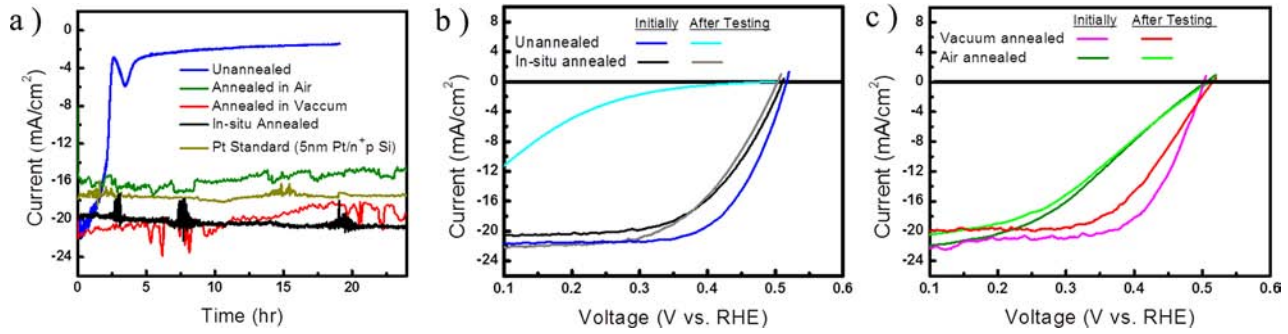

Figure 2. (a) Twenty-four hour tests of Pt/100 nm TiO_2/5 nm Ti on n^+p Si with various heat treatments. All samples were tested at +300 mV vs RHE. (b) CV's initially and after 24 h of testing of a vacuum annealed sample. (c) CV's initially and after 24 h of testing of an unannealed sample and an air-annealed sample. All samples were irradiated with the red part (λ > 635 nm) of the AM1.5 solar spectrum in an H_2-purged 1 M $HClO_4$ electrolyte.

(ISA). It should be noted over long times that the photoelectrochemical system would behave inconsistently, thus giving sharp peaks in the current. This is believed to be an effect of the irradiation source rather than the electrode.

Figure 2b shows the CV's of the UA and ISA samples initially and after 24 h of testing, while Figure 2c shows the CV's for the VA and AA samples. The initial and final CV's for the n^+p Si/5 nm Pt showed minimal change (SI, Figure S4).

Figure 2a clearly shows the importance of annealing on durability. The UA sample degrades relatively quickly and the VA sample has a slight degradation, while the ISA and AA samples show no noticeable degradation throughout the 24 h run. Given that the ISA sample had a better slope than the AA sample, the ISA sample was run for an additional 2 days (SI, Figure S5), without noticeable degradation. After testing, visual inspection showed the UA sample had all the TiO_2 removed, while the VA sample had some TiO_2 removed and the ISA and AA samples had none of the TiO_2 removed. SEM images of the initial and tested ISA and VA samples are shown in the Supporting Information (Figure S6). Recent work using a Cu_2O–TiO_2 photocathode has suggested that TiO_2 degradation could be due to formation of Ti^{3+} at highly reductive conditions.[17] In the current case, there is also the possibility that hydrogen atoms could penetrate the TiO_2 to react with underlying Ti to form a hydride.[18,19]

Sputter deposition at room temperature is typically known[20] to produce an amorphous material, which was verified in this case via XRD (SI, Figure S7). Heating the TiO_2 in a vacuum does provide enough thermodynamic driving force to allow the particles to rearrange, but XRD results show that this does not result in crystallinity. However, the XRD results of heating in air and in situ annealing both show crystallinity. This appears to be a key in understanding variations in durability.

Figure 2a shows rapid and slightly inconsistent degradation for the unannealed sample. Visual inspection after the experiment shows that all the TiO_2/Ti had been removed, thus explaining why this electrode had failed. Figure 2b shows that after testing the UA sample actually had an onset relatively close to the initial onset but a much worse slope. The two main determinants of the slope are the kinetics of the electrocatalysis and ohmic losses. Since Pt's Tafel slope is well-known and consistent with what we measure here,[21] it can be reasonably inferred that this slope difference is due to increased ohmic resistance related to SiO_2 formation.

By heating the sample to 400 °C, the TiO_2 should have enough thermal energy to rearrange itself in a more thermodynamically stable manner.[22] This should minimize the electrolyte attack on any defect ridden or highly strained TiO_2. The VA, AA, and ISA samples show that this treatment indeed helps to keep the TiO_2 attached, thus allowing the electrodes to have a steady photocurrent over the 24 h test. The slight reduction in CV slope after 24 h in Figure 2c suggests that there was some slight oxidation in the VA sample, thus indicating that the in situ annealed deposition procedure is probably a better procedure for durability.

The CV of the ISA sample shows a slightly worse CV, which is probably due to a slight oxidation of silicon from the deposition procedure. However, throughout the entire 72 h run (SI, Figure S5) there is no noticeable variation in the CVs, which shows the stability of this support. AFM images (SI, Figure S9) show that this is a much more rough surface than the vacuum-annealed sample, which allows oxidants to penetrate further into the TiO_2 network. However, the XRD shows that this is crystalline compared to the amorphous VA sample. The slight durability enhancement of the ISA sample over the VA sample indicates that crystallinity of the TiO_2 is more important for durability than a nonroughened surface.

Figure 2c shows that the AA sample had the same onset but a worse initial slope than the other samples. This explains why the long-term photocurrent in Figure 2a was lower in the AA sample compared to the VA sample. The difference in slope must be due to having air (e.g., oxygen) present during annealing. Since the TiO_2 is not a dense material, there is the potential for oxygen to diffuse through the 100 nm TiO_2. Heating to higher temperatures will only increase the diffusion as well as the potential to oxidize the remaining Ti (<5 nm) and possibly some Si. Oxidation of silicon would create an ohmic barrier, potentially explaining the decreased slope in Figure 2c. One other characteristic that annealing in air has over annealing in vacuum is that it can provide oxygen to fill any Ti^{3+} vacancies. This allows for the more compact crystalline anatase to form (SI, Figure S7), thus potentially explaining why there is very little difference in the before and after CV.

In general, Figure 2 shows that TiO_2 has the potential to provide long-term durability for the H_2 evolution on a photoabsorber, but also that optimizing processing conditions is quite important for long-term durability.

Band Diagram Analysis. With a device as complex as this, it is imperative that the band diagram of the device be understood. In the following work, an Fe(II)/Fe(III) redox couple is used to help understand the band diagram. A major goal of these experiments is to show that electrons are transferring through the TiO_2 conduction band rather than another mechanism. Mott–Schottky analysis (SI, Figure S10) indicates that the vacuum-annealed sample TiO_2 has a conduction band more reductive

dx.doi.org/10.1021/ja309523t | J. Am. Chem. Soc. 2013, 135, 1057–1064

than the H_2 evolution potential. Thus, one would expect there to be a significant barrier for electrons near the TiO_2/electrolyte interface until the Fermi level of the TiO_2 approaches that of the TiO_2 conduction band in aqueous solutions (−0.2 V vs RHE for anatase).[23] Interestingly, the photocurrents in Figure 1 show that this barrier at the TiO_2/electrolyte interface causes minimal overpotential loss in the H_2 evolution reaction. Using the Fe(II)/Fe(III) redox couple along with careful analysis of the band diagram of our system allows us to show why the TiO_2 is conductive enough at the H^+/H_2 redox potential to not cause any noticeable ohmic losses in unconcentrated solar illumination. Referring to previous dark electrochemical work done on TiO_2[13] helps us verify our understanding of the current band diagram.

The redox potential of Fe(II)/Fe(III) (in 1:1 ratio) is 0.77 V vs NHE. To verify this potential a Pt wire was cycled between −0.1 V and 1.4 V vs RHE in an argon-saturated 1 M $HClO_4$ solution with 10 mM each of iron(III) perchlorate and iron(II) perchlorate. The gray line in Figure 3a shows clear reduction and oxidation peaks around 0.77 V vs RHE from the Pt wire. The Pt wire's current was rescaled for ease in understanding. (The absolute current density of these peaks is irrelevant.) The addition of this redox pair to the electrolyte fixes the potential of the Pt at 0.77 V vs RHE, at least for low currents.

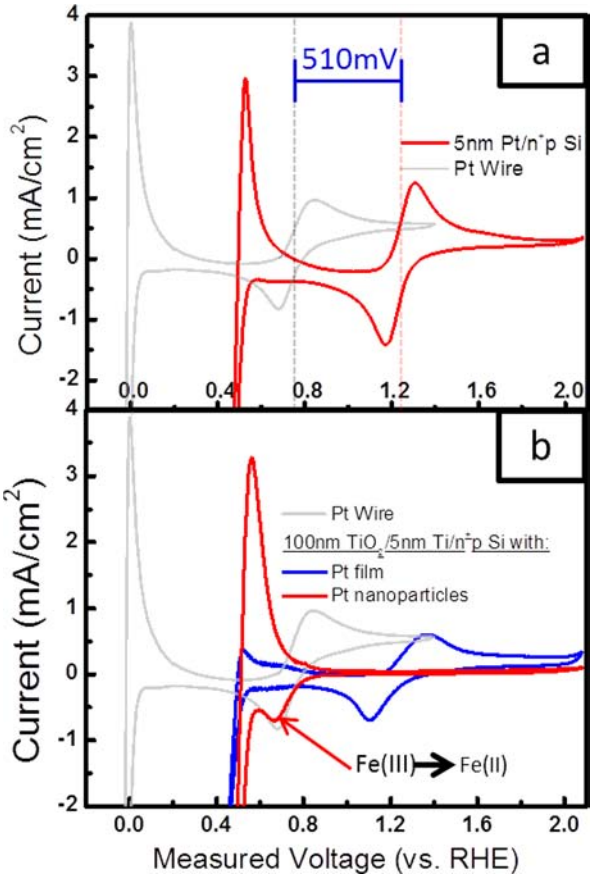

Figure 3. CV scans of a Pt wire and (a) sputtered 5 nm Pt/n^+p Si electrode and (b) a drop-cast Pt/100 nm TiO_2/5 nm Ti/n^+p Si electrode in an argon-purged 1 M $HClO_4$ electrolyte with 10 mM each of Fe(III) and Fe(II). The scan rate was 20 mV/s and the samples were irradiated with the red part (λ > 635 nm) of the AM1.5 spectrum.

To understand the photoelectrochemical characteristics of just the n^+p Si (without the Ti/TiO_2), an n^+p Si electrode with 5 nm of Pt sputtered on the surface was put into the same electrolyte. This electrode was then photoirradiated with the red part (λ > 635 nm) of AM1.5 solar spectrum while being cycled between 0.2 V vs RHE and 2.1 V vs RHE. The cyclic voltammogram in Figure 3a shows that the irradiated n^+p Si resulted in the Fe(II)/Fe(III) redox peaks being shifted anodically by ∼510 mV. Figure 3 shows the area of interest for this CV, while the entire CV is shown in the Supporting Information (Figure S11). While the H_2 evolution reaction takes place on platinum at 0.0 V vs RHE, this reaction on the illuminated n^+p Si/Pt electrode is also shifted ∼510 mV anodically.

Figure 4 shows schematically why both the Fe(II)/Fe(III) and H^+/H_2 reactions are shifted by 510 mV. Figure 4a shows the 5 nm Pt/n^+p Si electrode in the dark when the electrode is set at a potential of 0.0 V vs RHE. This potential sets the Fermi level (dotted line) throughout the silicon in Figure 4. In the dark the p−n junction diode has an extremely low conductance, which will prevent reduction currents and severely limit oxidation currents, i.e., no activity. When this sample is irradiated in Figure 4b, photogenerated electron−hole pairs are produced. The electron−hole pairs are separated by the built-in electric field in the p−n junction, which drives the electrons to the n^+ layer while the holes flow to the p-type layer. As a result, a photovoltage is created and the differential conductance of the junction is dramatically increased (∼8−9 orders of magnitude). As the Lewis group has shown,[24] the n^+p Si creates an internal band-bending, which results in a consistent photovoltage that is independent of electrolyte interactions. In situations where silicon at the surface is highly doped (e.g., the n^+ layer), Pt is known to form an ohmic contact.[14] Thus, the potential of the Pt will be almost identical to that of the n^+ layer.

Parts b and c of Figure 4 show the 5 nm Pt/n^+p Si electrode under illumination at 0.51 and 1.28 V vs RHE, respectively. For both of these illuminated electrodes a photovoltage, i.e., a separation of electron and hole quasi-Fermi levels, is present. As a result, the Fermi level of the back contact of the sample and the Pt Fermi level differ by the photovoltage, as illustrated. In experiments the potentiostat measures or controls the potential of the back contact, i.e., the position of that Fermi level. For the electrochemistry, however, the position of the Pt Fermi level is what matters, since the Pt is in contact with the electrolyte. Once the photovoltage is known, the potentials read from the potentiostat may be compensated for the photovoltage to reflect the potential of the electrode at the electrolyte interface (in the present case the potential of Pt).

In the case of the 5 nm Pt/n^+p Si electrode, the difference in measured potential for the Fe(III)/Fe(II) or H^+/H_2 redox reactions and the respective literature values (+0.77 or 0.0 V vs RHE, respectively) is used to determine the photovoltage (both reactions give a value of 0.51 V). Schematically this can be seen in Figure 4b,c. Once the photovoltage is subtracted from the potentiostat potentials, this experiment may be treated as a purely electrochemical experiment in the low-current limit (were the optical excitation rate ≫ external current). Now that the n^+p Si system is understood, the effects of Ti/TiO_2 can be investigated.

The bottom graph in Figure 3 shows two vacuum-annealed Pt/100 nm TiO_2/5 nm Ti/n^+p Si electrodes photoirradiated and cycled under the same conditions as the 5 nm Pt/n^+p Si electrode, with the Pt wire CV also being shown for reference purposes. The difference between the two samples is that the sample denoted by the blue line consists of a 5 nm sputtered Pt covering 100% of the surface while the sample for the red line consists of Pt nanoparticles covering ∼20% of the surface. The

dx.doi.org/10.1021/ja309523t | J. Am. Chem. Soc. 2013, 135, 1057−1064

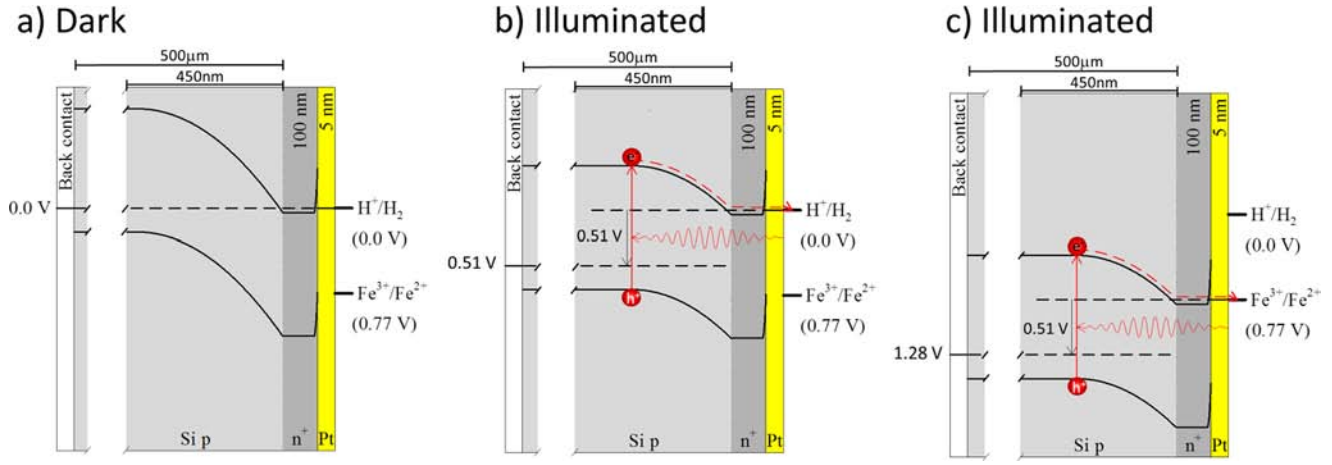

Figure 4. Schematic energy levels of an n^+p Si/5 nm Pt (a) in the dark in equilibrium with the H^+/H_2 reaction, (b) illuminated at 0.51 V vs RHE, thus driving the $2H^+ \rightarrow H_2$ reaction, and (c) illuminated at 1.28 V vs RHE, thus driving the $Fe^{3+} + e^- \rightarrow Fe^{2+}$ reaction.

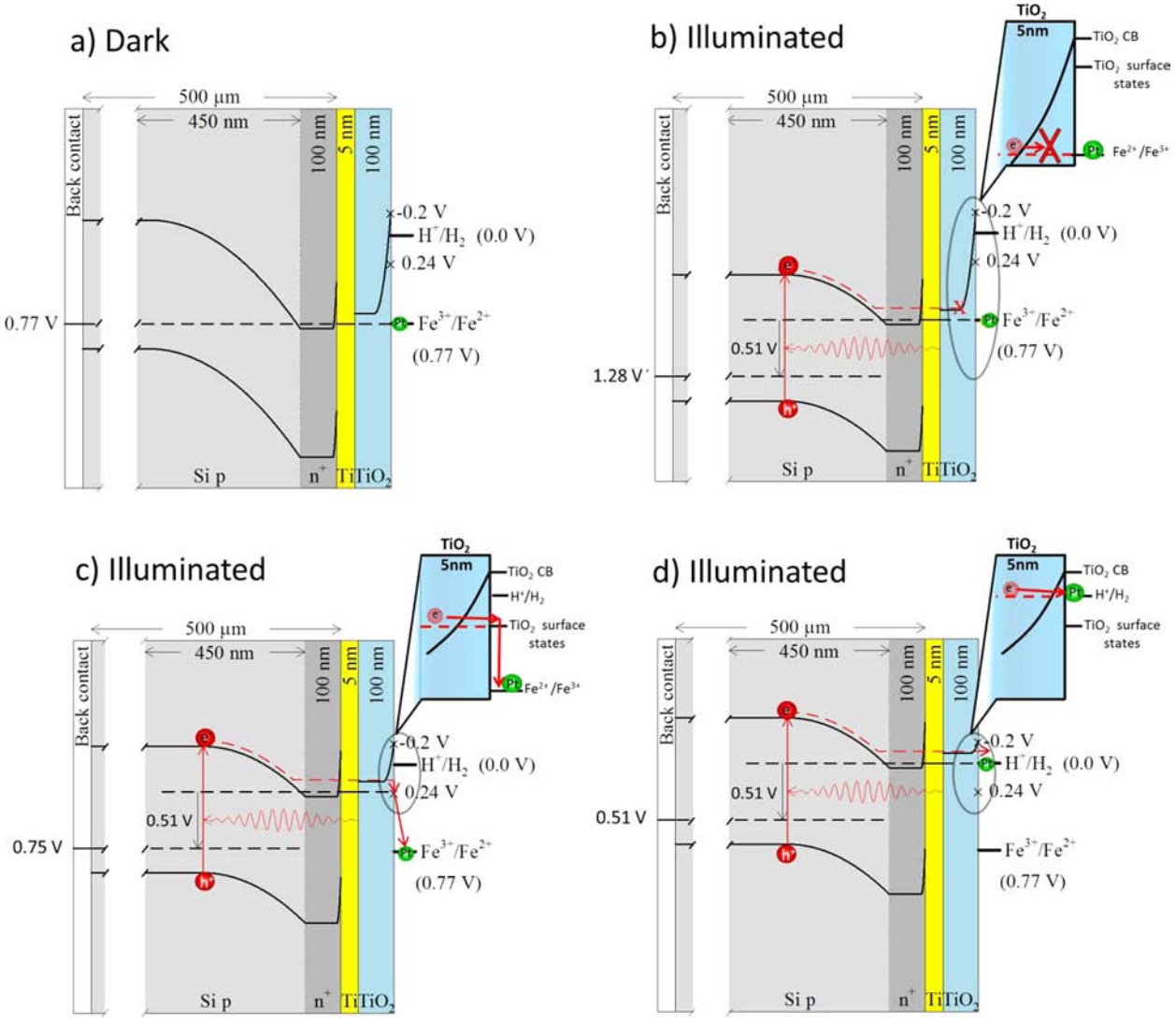

Figure 5. Schematic energy levels of the n^+p Si with 5 nm Ti/100 nm TiO_2 (a) in the dark at 0.77 V vs NHE in equilibrium with Fe^{2+}/Fe^{3+}, (b) illuminated at 1.28 V vs RHE in quasi-equilibrium with Fe^{2+}/Fe^{3+}, (c) illuminated at 0.75 V vs RHE, thus driving the $Fe^{3+} + e^- \rightarrow Fe^{2+}$ reaction, and (d) illuminated at 0.51 V vs RHE, thus driving the $2e^- + 2H^+ \rightarrow H_2$ reaction.

important difference between these samples is that in the sputtered film case the TiO_2 does not see the electrolyte, while in the nanoparticle case the TiO_2 does see and interact with the electrolyte.

dx.doi.org/10.1021/ja309523t | J. Am. Chem. Soc. 2013, 135, 1057−1064

It should be noted that in Figure 3 the samples were illuminated with red light; thus, the TiO_2 was not photoirradiated with photon energies above the band gap. In terms of analyzing this electrode, TiO_2 can be thought of as acting as a semiconductor in the dark.

Figure 3b shows that the CV of the Pt film deposited on TiO_2 looks similar to the Pt film without TiO_2, with an obvious reduction and oxidation of the Fe ions. The H_2 reduction onset appears to be slightly shifted, with the H_2 oxidation peak noticeable, but much smaller. The smaller H_2 oxidation peak can simply be attributed to differences in surface morphology (see SI, Figure S11). Reviewing the band diagrams in Figure 4, the only difference with the case of the Pt film on the 100 nm TiO_2/5 nm Ti/n^+p Si electrode is that there is Ti and TiO_2 between the silicon and Pt. It would be expected that Ti on n^+ Si would act similar to Pt and form an ohmic contact. The TiO_2 should simply act as a resistor that is a function of the Ti/TiO_2 interface, TiO_2 dopant density, and TiO_2/Pt interface. Thus, given the similarities in band diagrams between the Pt film on 100 nm TiO_2/5 nm Ti/n^+p Si and 5 nm Pt/n^+p Si, it is easy to see why these two electrodes behave similarly when photoirradiated in the acidic Fe(II)/Fe(III) electrolyte.

Figure 3b shows that the electrodes with Pt nanoparticles behave much differently than the electrode with a Pt film. The electrode with Pt nanoparticles show no Fe(II) oxidation and a shifted Fe(III) reduction peak, but generally the same H_2 oxidation and reduction peak. The only major difference between the Pt film and Pt nanoparticles is that, in the Pt nanoparticle case, the TiO_2 interacts with the electrolyte. This interaction is known to pin the conduction band level of the TiO_2 at a given potential,[23] which leads to the drastic change in the electrodes interaction with the Fe(II)/Fe(III) redox couple. The band diagram for this system must be looked at to help one understand the results from Figure 3b. First, however, the conduction band and dopant density of TiO_2 in the electrolyte must be calculated.

To determine the conduction band position as well as dopant density, Mott–Schottky characterization was employed on an equivalent (e.g., no p–n junction) vacuum-annealed sample (SI, Figure S10) without Pt. This resulted in a conduction band of −0.23 V vs RHE and a dopant density of 3×10^{17} cm^{-3}. With these two values a band diagram of the electrode can now be developed.

Figure 5a shows the electrode in the dark at a bias of 0.77 V vs RHE. This bias then sets the Fermi level (dotted line) throughout the electrode. Exactly as in Figure 4a, the n^+p Si diode in the dark prevents significant oxidative and reductive currents. The titanium metal, like Pt, forms an ohmic contact to the n^+ layer in the potential range of the cyclic voltammogram. From the Mott–Schottky results the conduction band can be drawn at −0.23 V vs RHE. To match the Fermi level of the system, the bulk TiO_2 conduction band will be strongly bent, as shown in Figure 5a; using the dopant density, the depletion layer thickness can be calculated as a function of voltage (see SI). This allows for the depletion layer through the TiO_2 to be drawn in Figure 5a–d.

It should be restated that in this case we have Pt nanoparticles rather than a Pt film, resulting in the TiO_2 directly interacting with the electrolyte. This entails that the energetics of the system will most likely be based on the TiO_2/electrolyte interface, and hence the Pt is "pinched off" from the band diagram.[25] This isolation from the electrode allows the energy level of the Pt to equilibrate with that of the dominating redox species in the electrolyte. Figure 5b shows the composite illuminated. If there were just the n^+p Si without the Ti/TiO_2, the added photovoltage of ∼0.51 V should allow for the potential at the surface/electrolyte interface to be reductive enough to reduce Fe(III) to Fe(II). While in the case with a Pt electrode this reaction occurs (See Figure 3a and 4b), Figure 5b shows that the pinning of the TiO_2 layer at the electrolyte interface creates a barrier for the electrons. The electrons do not have the energy to climb this barrier, thus explaining why there is no current at this potential in Figure 3b. So while the thermodynamics of the Fe(III) reduction is favorable, this reaction cannot occur until the barrier of the TiO_2 pinning level is overcome. This semiconducting barrier effect has been seen in the past,[13] albeit without the n^+p Si photoabsorber.

Figure 3b shows that there is no reductive current until ∼0.7 V vs RHE. At this point the electrons are at a potential reductive enough that they are not limited by the pinning of the TiO_2, which then allows them to flow through the TiO_2 to reduce Fe(III) to Fe(II), as illustrated in Figure 5c. (It is simply coincidence that the Fe(III) reduction on TiO_2 takes place at the same potential as the Pt wire.) While it is apparent that the Fe(III) reduces to Fe(II) when the potentiostat is at 0.7 V vs RHE, the more important question is what the actual potential across the surface/electrolyte interface is when this reduction occurs. To find this potential, the photovoltage needs to be found and then subtracted from the potential applied by the potentiostat. Figure 3b shows that the reversible H^+/H_2 redox reaction occurs at a potential of 0.51 V vs RHE. Since the equilibrium potential for this reaction is 0.0 V, the photovoltage for the Pt/100 nm TiO_2/5 nm Ti/n^+p Si can be estimated to be 0.51 V vs RHE. This is based on the assumption that there is negligible voltage loss through the 100 nm of TiO_2. The fact that the determined photovoltage is actually slightly higher than the case for the 5 nm Pt/n^+p Si supports this assumption. (The slight increase in photovoltage may be due to reduced surface recombination when Ti/TiO_2 borders Si instead of Pt.)

Compensating for photovoltage, it is apparent that the Fe(III) starts to reduce to Fe(II) at 0.24 V vs RHE. This onset potential of Fe(III) would suggest that this pre-flat-band current is due to surface states. This pre-flat-band current from TiO_2 surface states has been seen by many authors and has been shown to start as early as 450 mV before the flat-band potential.[13,26,27] Vandermolen et al. explained this effect by showing that even with band-bending there is a small population of conduction band electrons at the surface/electrolyte interface that can depopulate into surface states.[27] While Vandermolen's approach has been generally accepted,[26] tunneling also can occur, and Vanmaekelbergh did an in-depth study of the relative rates between tunneling and depopulation from the conduction band.[28] It is beyond the scope of this work to determine the exact mechanism for electron transfer to the surface states. Thus, in Figure 5c,d the electron is shown traveling through to the surface states using tunneling, but the actual mechanism might be much more complex.

Figure 5d shows the electrode potential in the case where the voltage at the semiconductor/electrolyte interface is more reductive than the H_2 evolution reaction. While in the figure only the H_2 evolution reaction is being illustrated, in actuality both the Fe(III) and H^+ are being reduced simultaneously. However, the electrolyte contains 1 M H^+ and 10 mM Fe(III), so it is assumed that the H_2 evolution reaction will dominate. The drastic increase in electrode current verifies this (SI, Figure S11). The true potential of the Pt is also hard to know, but since the H_2

dx.doi.org/10.1021/ja309523t | J. Am. Chem. Soc. 2013, 135, 1057–1064

evolution is the dominating reaction, the average Pt particle's potential will most likely lie near that of the H^+/H_2 evolution reaction.

The H^+/H_2 redox reaction in Figure 3b also divulges some interesting information about the system. On the cathodic scan the electrode first reduces Fe(III) and then reduces the H^+ to H_2. The Fe(III) reduction at 0.2 V vs RHE is important because it shows the onset potential at which electrons can travel through TiO_2. Figure 5d illustrates that since the H^+/H_2 redox potential is more cathodic than 0.2 V vs RHE, this reaction should not be limited by a lack of TiO_2 electronic states to travel through. Since TiO_2 has a conduction band rather than a single electronic state, there will be a large density of states at these reductive potentials. Thus, the TiO_2 will act metallic and will actually go into accumulation as the potential cycles to more cathodic potentials. This answers the initial question: Why there were no overpotential losses in Figure 1 relating to the difference between the TiO_2 conduction band and the H^+/H_2 redox couple.

The H_2 oxidation also reveals intricacies of the system. In Figure 3b, the anodic scan shows an H_2 oxidation peak slightly anodic of the open circuit potential (e.g., 0.0 V vs RHE at the semiconductor/electrolyte interface). This peak decreases due to all the H_2 in the vicinity of the surface becoming oxidized, and the argon purging prevents any more H_2 from reaching the surface. Figure 6 focuses on this reaction by taking either a 5 nm Pt/n^+p Si

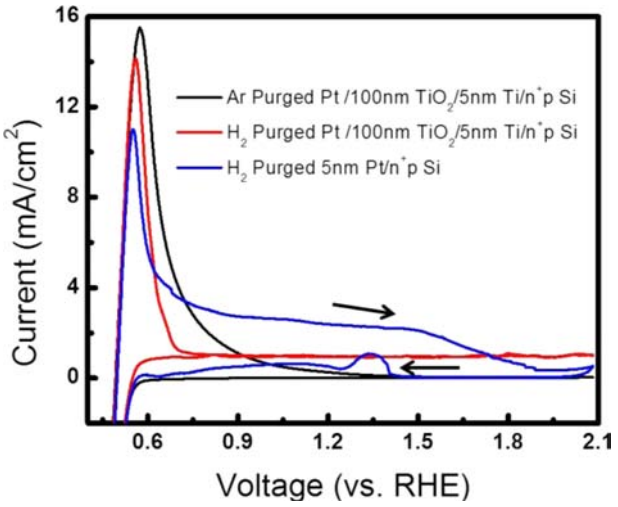

Figure 6. CV scans of a red light (λ > 635 nm) irradiated Pt/100 nm TiO_2/5 nm Ti/n^+p Si electrode in an electrolyte with 1 M $HClO_4$ at 50 mV/s. The sample was first bubbled in argon and then in H_2 to show the effect of the H_2 oxidation reaction.

or a Pt nanoparticle/100 nm TiO_2/5 nm Ti/n^+p Si electrode and cycling it between −0.1 and 2.1 V vs RHE in a 1 M $HClO_4$ solution. While Figure 6 focuses on the area of interest, the entire CV is shown in the Supporting Information (Figure S12). It should be noted that the Fe(III)/Fe(II) redox couple was removed to simplify the system. In the Supporting Information (Figure S13) the case where both the H^+/H_2 and Fe(III)/Fe(II) are in solution is shown and explained. It should be noted that in all these experiments it was discovered that the exact H_2 oxidation current was a function of how vigorously the solution was bubbled with H_2, thus indicating that this is a mass-transfer-limited process.

By looking at the Pt on TiO_2 sample in Figure 6, it shows that H_2 can be oxidized even at surface/electrolyte potentials anodic of the surface states of the TiO_2. The energy diagram of Figure 5c can again be looked at to understand this process. Since the H^+/H_2 redox potential is slightly more reductive than the TiO_2 surface states, electrons can transfer to the surface states and then on into the conduction band, or they may tunnel directly into the conduction band. Once the electrons are in the TiO_2, the band-bending is favorable to transfer them through the TiO_2 to the Ti and onto the Si, where they will recombine with photogenerated holes.

In Figure 3b the TiO_2-protected electrode is in an Fe(II)/Fe(III) solution, and it is clear that the electrode cannot oxidize the Fe(II) to Fe(III), since there is no current at this redox potential. Figure 5c helps to clarify why this is the case. Since the TiO_2 conduction band is pinned at −0.2 V vs RHE in this system, the Fe(II) would have to either tunnel through the depletion layer (138 nm) or increase in energy up in energy to the TiO_2 surface states if it were to be reduced. Both cases are highly unlikely, thus explaining the lack of Fe(II) oxidation current in Figure 3b. It is interesting that since the Fe(II)/Fe(III) redox potential is oxidative of the TiO_2 conduction band/surface states, the TiO_2 will always act as an electrical insulator for this oxidation reaction. However, in the case of the H^+/H_2, the redox potential is more reductive than the TiO_2 surface states; thus, TiO_2 will always act as an electrical conductor for this reaction.

Looking at what happens to the 5 nm Pt/n^+p Si in Figure 6 is also interesting. It can be seen that on the anodic peak the H_2 current starts to quickly drop at 1.5 V vs RHE, and on the cathodic peak there is a hump near 1.3 V vs RHE. If we take the ~510 mV photovoltage into consideration, this tells us that the Pt surface is actually at 1.0 V vs RHE when the H_2 declines on the anodic peak and at 0.8 V vs RHE when the hump occurs on the cathodic peak. Both of these effects can be explained by the fact that Pt oxidizes to form Pt oxide at a redox potential (1.0 V vs RHE).[21] Since platinum oxide does not oxidize H_2,[29] the decrease in H_2 oxidation in the anodic scan at 1.5 V can be attributed to the formation of the Pt oxide. On the cathodic scan the hump at 1.3 V vs RHE can be attributed to the reduction of Pt oxide back to metallic Pt and the subsequent H_2 oxidation associated with it.

While the Pt/Pt oxide redox reaction is clearly visible in the case with 5 nm Pt/n^+p Si, this redox reaction is not seen in the Pt/100 nm TiO_2/5 nm Ti/n^+p Si electrode. The reason the Pt oxidation does not occur on the TiO_2 sample is the same as for the Fe(II) species: The position of the TiO_2 conduction band/surface states creates a barrier, preventing oxidation.

This photocathode's inability to oxidize anodic of 0.2 V vs RHE can be quite useful if an H_2 evolution catalyst is developed that has stability issues with oxidation. As long as the oxidation potential of any catalyst is anodic of the TiO_2 surface states, the catalyst will not risk being oxidized by the electrode. On the other hand, the inability of the TiO_2-capped electrode to drive oxidation on its surface becomes an issue if the catalyst needs to be electrodeposited in an anodic process. In the case of the amorphous MoS_x catalyst originally developed by the Hu group,[30] the catalyst is deposited by cycling to potentials as oxidative as 0.75 V vs RHE. It was clear that the Fe(II) with a redox potential of 0.77 V vs RHE could not oxidize; thus, it would not be expected for this deposition to occur. Using an approach similar to our previous work,[12] we tried the deposition of the amorphous MoS_x catalyst and, as expected, the cycling fails at the oxidative step, and thus, the catalyst did not deposit (not shown). Our current research is focusing on attaching other Mo-based H_2

dx.doi.org/10.1021/ja309523t | J. Am. Chem. Soc. 2013, 135, 1057−1064

evolution catalysts to this system to study the long-term durability effects of these systems.

CONCLUSION

In conclusion, we showed that TiO_2 can be used as an intermediate between a photoabsorber and a catalyst with negligible resistance and a >72 h stability under HER at pH 0. By optimizing the deposition procedure, the protection layer can be quite resistant to any degradation in performance. The investigation with the Fe(II)/Fe(III) redox couple helps to verify that the electron is transferring through the conduction band. This experiment also gives insight into the unique features that result from electron transfer through a conduction band as compared to a metal such as Pt.

ASSOCIATED CONTENT

Supporting Information

Experimental details and more detailed cyclic voltammograms and chronoampometry experiments are shown, as well as microscopic images, XRD, and IPCE experiments. This material is available free of charge via the Internet at http://pubs.acs.org.

AUTHOR INFORMATION

Corresponding Author

ibchork@fysik.dtu.dk

Notes

The authors declare no competing financial interests.

ACKNOWLEDGMENTS

We gratefully acknowledge the Danish Ministry of Science for funding the CAtalysis for Sustainable Energy (CASE) initiative, the Danish National Research Foundation for funding The Center for Individual Nanoparticle Functionality (CINF).

REFERENCES

(1) Kamat, P. V. *J. Phys. Chem. C* **2007**, *111*, 2834.
(2) Lewis, N. S.; Nocera, D. G. *Proc. Natl. Acad. Sci. U.S.A.* **2006**, *103*, 15729.
(3) James, B.; Baum, G.; Perez, J.; Baum, K. *Technoeconomic Analysis of Photoelectrochemical (PEC) Hydrogen Production*; Technical Report; Directed Technologies: Arlington, VA, 2009.
(4) Dahl, S.; Chorkendorff, I. *Nat. Mater.* **2012**, *11*, 100.
(5) Kudo, A.; Miseki, Y. *Chem. Soc. Rev.* **2009**, *38*, 253.
(6) Hou, Y.; Abrams, B. L.; Vesborg, P. C. K.; Bjorketun, M. E.; Herbst, K.; Bech, L.; Setti, A. M.; Damsgaard, C. D.; Pedersen, T.; Hansen, O.; Rossmeisl, J.; Dahl, S.; Norskov, J. K.; Chorkendorff, I. *Nat. Mater.* **2011**, *10*, 434.
(7) Weber, M. F.; Dignam, M. J. *Int. J. Hydrogen Energy* **1986**, *11*, 225.
(8) Laursen, A. B.; Kegnaes, S.; Dahl, S.; Chorkendorff, I. *Energy Environ. Sci.* **2012**, 5.
(9) Castelli, I.; Landis, D.; Thygesen, K.; Dahl, S.; Chorkendorff, I.; Jaramillo, T.; Jacobsen, K. *Energy Environ. Sci.* **2012**, *5*, 9034.
(10) Haick, H.; Hurley, P. T.; Hochbaum, A. I.; Yang, P.; Lewis, N. S. *J. Am. Chem. Soc.* **2006**, *128*, 8990.
(11) O'Leary, L. E.; Johansson, E.; Brunschwig, B. S.; Lewis, N. S. *J. Phys. Chem. B* **2010**, *114*, 14298.
(12) Seger, B.; Laursen, A. B.; Vesborg, P. C. K.; Pedersen, T.; Hansen, O.; Dahl, S.; Chorkendorff, I. *Angew. Chem.* **2012**, *51*, 9128.
(13) Noufi, R. N.; Kohl, P. A.; Frank, S. N.; Bard, A. J. *J. Electrochem. Soc.* **1978**, *125*, 246.
(14) Boettcher, S. W.; Warren, E. L.; Putnam, M. C.; Santori, E. A.; Turner-Evans, D.; Kelzenberg, M. D.; Walter, M. G.; McKone, J. R.; Brunschwig, B. S.; Atwater, H. A.; Lewis, N. S. *J. Am. Chem. Soc.* **2011**, *133*, 1216.
(15) Richards, B. S. *Prog. Photovoltaics* **2004**, *12*, 253.
(16) Ohtsuka, T.; Masuda, M.; Sato, N. *J. Electrochem. Soc.* **1985**, *132*, 787.
(17) Paracchino, A.; Mathews, N.; Hisatomi, T.; Stefik, M.; Tilley, S. D.; Gratzel, M. *Energy Environ. Sci.* **2012**, *5*, 8673.
(18) Zhang, H.; Kisi, E. H. *J. Phys.: Condens. Matter* **1997**, *9*, L185.
(19) Libowitz, G. G. *J. Nucl. Mater.* **1960**, *2*, 1.
(20) Suhail, M. H.; Rao, G. M.; Mohan, S. *J. Appl. Phys.* **1992**, *71*, 1421.
(21) Markovic, N. M.; Grgur, B. N.; Ross, P. N. *J. Phys. Chem. B* **1997**, *101*, 5405.
(22) Vives, S.; Meunier, C. *Thin Solid Films* **2010**, *518*, 3748.
(23) Fujishima, A.; Zhang, X.; Tryk, D. A. *Surf. Sci. Rep.* **2008**, *63*, 515.
(24) Warren, E. L.; Boettcher, S. W.; Walter, M. G.; Atwater, H. A.; Lewis, N. S. *J. Phys. Chem. C* **2011**, *115*, 594.
(25) Walter, M. G.; Warren, E. L.; McKone, J. R.; Boettcher, S. W.; Mi, Q.; Santori, E. A.; Lewis, N. S. *Chem. Rev.* **2010**, 110.
(26) Rajeshwar, K. *Encyclopedia of Electrochemistry. Semiconductor Electrodes and Photoelectrochemistry*; Wiley: New York, 2002; Vol. *6*.
(27) Vandermolen, J.; Gomes, W. P.; Cardon, F. *J. Electrochem. Soc.* **1980**, *127*, 324.
(28) Vanmaekelbergh, D. *Electrochim. Acta* **1997**, 42.
(29) Barz, F.; Lungu, M. *J. Electroanal. Chem.* **1982**, *133*, 101.
(30) Merki, D.; Fierro, S.; Vrubel, H.; Hu, X. *Chem. Sci.* **2011**, *2*, 1262.